Available online at www.sciencedirect.com

ScienceDirect

Physics Procedia 83 (2016) 1377 – 1386

Physics Procedia

9th International Conference on Photonic Technologies - LANE 2016

Numerical simulation of the thermal efficiency during laser deep penetration welding

A. Ganser[a,*], J. Pieper[a], S. Liebl[a], M. F. Zaeh[a]

[a]*Institute for Machine Tools and Industrial Management (iwb), Technical University of Munich, Boltzmannstraße 15, 85748 Garching, Germany*

Abstract

The advantages of laser beam welding, such as its high flexibility, its high local energy input, and its fast processing speed, led to a substantial increase of industrial applications of the technology. High losses can be observed during laser welding of materials with a high thermal conductivity, such as aluminum or copper. This is caused by the heat conduction losses in the surrounding area of the process zone and due to reflections. These energy losses lead to a reduced efficiency of the laser welding process.
A numerical model based on a CFD simulation is presented, which enables to calculate the molten pool isotherms. The thermal efficiency is determined for different keyhole geometries and welding velocities. This efficiency is defined as the ratio between the energy which is required to melt the volume of metal in the fusion zone and the absorbed laser beam power.

Peer-review under responsibility of the Bayerisches Laserzentrum GmbH

Keywords: CFD simulation; efficiency; laser welding; copper

1. Introduction

Laser beam welding is an established joining technology because of its great flexibility and its high degree of automation. Due to the development of high power laser sources, this technique is also used for the welding of non-

* Corresponding author. Tel.: +49-89-289-15539; fax: +49-89-289-15555 .
E-mail address: Andreas.Ganser@iwb.tum.de

Peer-review under responsibility of the Bayerisches Laserzentrum GmbH
doi:10.1016/j.phpro.2016.08.144

ferrous metals. During laser beam welding of copper materials, high energy losses are observed caused by the high reflectivity and the high thermal conductivity [1]. To reduce the energy losses caused by reflections, laser radiation in the green spectral range can be used [2]. In contrast, there is no technical solution to decrease energy losses caused by the high thermal conductivity. However, the thermal efficiency can be improved by an appropriate setting of process parameters.

This paper presents a numerical 3D model to determine the thermal efficiency of a laser beam welding process based on a CFD simulation. Therefore, the influence of the laser beam power, the focus diameter of the laser beam, and the welding speed on the thermal efficiency during laser beam welding of copper materials is analyzed.

2. State of the Art

2.1. Calculation of the thermal efficiency with analytical methods

The thermal efficiency η_{th} is defined as the ratio of the power required for melting the volume of metal in the fusion zone P_{th} and the absorbed laser beam power P_A [3] and is described by:

$$\eta_{th} = \frac{P_{th}}{P_A} = \frac{A \cdot \rho \cdot v \cdot \left(c_p \cdot \left(T_M - T_A\right) + h_M\right)}{P_A}, \tag{1}$$

where A is the area of the cross section of the molten pool, ρ the density, v the welding speed, c_p the specific heat capacity, T_M the melting temperature, T_A the ambient temperature, and h_M the latent heat for melting. Using equation (1) it have to be considered, that the energy for heating the material outside of the molten pool as well as the energy for overheating the molten pool are assumed to be energy losses.

There are several approaches to calculate the maximum of the thermal efficiency during laser beam welding. All models base on the heat conduction equations and are used to calculate the melting area. To obtain the thermal efficiency during a heat conduction welding process, the point-source model is suitable [3]. In this model, a semi-infinite body is assumed. The laser energy is applied pointwise and the source is moved on the surface of the workpiece. The heat conduction propagates in radial direction in the model, so the melting area can be described by a half circle and calculated for a stationary state. Therefore, the theoretical thermal efficiency results in a maximum of 36.8 %. For calculating the thermal efficiency during a full penetration welding process, a moving line source can be used [3]. In this case, the heat conduction in the normal direction to the surface is insignificant, so that only heat conduction in radial direction to the line source has to be considered. This leads to a rectangular cross section of the molten pool with a maximum theoretical thermal efficiency of 48.4 %.

SWIFT-HOOK AND GICK [4] use a normed and dimensionless welding speed and power for the calculation of the thermal efficiency. By assuming a moving line source they could also determine a maximum thermal efficiency of 48.4 %.

To incorporate the dimension and the shape of the keyhole, an integrated point-source model was used by CHANG ET AL. [5]. This model is based on the idea, that each point of the keyhole surface can be described as a point source. Using this model, a parabolic cross section could be obtained, since the different isotherms of each point source are overlapping. This provides also a maximum theoretical thermal efficiency of 48.4%.

All of these models are based on analytic considerations regarding heat conduction. They do not include fluid flow and latent heat and they have a limited validity in terms of the welding speed. To take this into account, numerical models can be used to calculate the molten pool geometry. These models are introduced below.

2.2. Numerical process models

A common method for the numerical simulation of laser beam welding processes is the Volume-of-Fluid method (VOF). This method allows to simulate the formation of a keyhole. To include the welding speed, a three-dimensional model must be used. This enables the determination of the molten pool´s cross section during laser beam welding [6, 7, 8]. Since the main focus of these models is on the formation of the keyhole, they are very

complex and associated with a very long computing time. To obtain the thermal efficiency, only the cross section of the molten pool has to be identified. For this purpose, a numerical model with a predefined keyhole geometry can be applied.

To evaluate the impact of electromagnetic stirring on the element distribution in laser beam welding, GATZEN ET AL. [9] used a numerical model with a predefined keyhole geometry. The following simplifications are assumed:

- Laminar and incompressible fluid flow
- Predefined keyhole and model geometry
- Evaporation temperature at the keyhole surface
- Consideration of the melt enthalpy using a modified heat capacity

The Marangoni convection, the fluid flow in the liquid phase driven by the metal vapor, and the thermal convection are considered in this model. It was shown, that the vapor driven fluid flow and the Marangoni convection have a major influence on the geometry of the molten pool. Both effects result in a wider molten pool of the surface.

BACHMANN ET AL. [10] analyzed the effect of oscillating magnetic fields on the process stability during laser beam welding of non-magnetic materials. For this purpose, a numerical model with a predefined keyhole geometry was used. In this model, the thermal and the Marangoni convection are considered, while the fluid flow induced by the outflow of the metal vapor of the keyhole is neglected. It was shown, that the thermal convection driven by density differences has a very small influence on the melting zone.

3. Objective and Approach

As shown above, there are different analytical models to determine the thermal efficiency during keyhole welding. These models operate with significant simplifications for the heat source and without considering the fluid flow in the molten pool. Due to the high reflectivity of copper materials for infrared laser radiation of common laser beam sources like fiber laser or disk lasers, an appropriate determination of the welding parameters is important to guarantee an efficient welding process. For this reason, a numerical approach to predict the thermal efficiency of a keyhole welding process depending on the keyhole geometry and the welding velocity is presented.

The numerical model is based on a heat input by a predefined, stationary keyhole geometry and includes both, three-dimensional heat conduction and fluid flow. In addition, thermal convection, Marangoni convection, and convection caused by metal vapor, which streams out of the capillary, are considered. For modeling the phase transformation and the fluid flow, temperature-dependent material properties are taken into account. In a next step, the numerical model was validated by comparison with experimental analysis. Finally, the calculation and evaluation of the thermal efficiency during laser welding of copper material using the numerical model is presented for different process parameters.

4. Numerical model

4.1. Basic equations

Regarding a laminar and incompressible fluid flow, the conservation equations of mass (2), momentum (3), and energy (4) need to be solved in the solid and liquid phase and they can be written as follows:

$$\frac{\partial \rho}{\partial t} + \nabla\left(\rho \cdot \vec{u}\right) = 0 \tag{2}$$

$$\rho\left(\frac{\partial \vec{u}}{\partial t} + \left(\vec{u} \cdot \nabla\right)\vec{u}\right) = \vec{k} - \nabla p + \eta \cdot \Delta \vec{u} \tag{3}$$

$$\lambda \cdot \Delta T + \dot{\omega} = \rho \cdot c_p \cdot \frac{\partial T}{\partial t} + \nabla\left(\rho \cdot c_p \cdot T(\vec{x},t) \cdot \vec{u}\right) \tag{4}$$

ρ describes the density, $\vec{u}$ the velocity vector, $\vec{k}$ the volume force, p the pressure, η the dynamic viscosity, λ the thermal conductivity, T the temperature, $\dot{\omega}$ the heat source density, and c_p the specific heat capacity. The separation of the solid and liquid phase is controlled by the temperature-dependent dynamic viscosity η. For the solid phase a high value is used for the dynamic viscosity, hence the fluid reacts like a solid.

4.2. Implemented fluid convections

Besides the heat conduction, also the fluid flow is considered for the calculation of the geometry of the molten pool. The fluid flow in the molten pool is driven by the following effects:

- Thermal convection
- Marangoni convection
- Convection through emerging metal vapor in the keyhole
- Fluid flow around the keyhole

While the thermal and the Marangoni convection as well as the convection driven by emerging metal vapor in the keyhole have to be implemented using special boundary conditions, the fluid flow around the keyhole occurs by itself if a welding velocity is considered.

Thermal convection

In the basic equations (2) – (4) a constant and temperature-independent density is assumed. Therefore, no thermal convection would occur. Nevertheless, this convection is taken into account by a volume force $\vec{k}_{thermal}$ in equation (3), given by:

$$\vec{k}_{thermal} = \begin{cases} 0 & T < T_M \\ \left(\rho + \alpha \cdot \left(T - T_M\right)\right) \cdot \vec{g} & T >= T_{M,} \end{cases} \tag{5}$$

where α is the thermal coefficient of expansion, T_M the melting temperature and $\vec{g}$ the gravity constant.

Marangoni convection

Induced by different temperatures a gradient in the surface tension occurs, which leads to a stress at the surface of the molten pool. As a consequence of that a fluid flow in the direction of the higher surface tension occurs [11]. This is known as the Marangoni convection. The stress $\vec{\tau}_{MK}$ can be described by:

$$\vec{\tau}_{MK} = \nabla\gamma = \frac{\partial\gamma}{\partial T}\nabla T \tag{6}$$

For pure substances the gradient of the surface tension γ is constant ($\partial y/\partial T$ = constant), so that only the gradient of the temperature has to be known for calculating the stress [12]. This stress is implemented in the model as a boundary condition on the top of the molten pool as a weak contribution in the equation of the conservation of the momentum (2).

Convection induced by evaporation of metal

The material in the keyhole is vaporized continuously. The metal vapor streams upwards within the keyhole and generates a stress on the keyhole´s wall. For a laminar pipe flow by Hagen-Poiseuille [13] and with the Newton-stress-law the shear-stress τ can be calculated by:

$$\tau = \mu \cdot \frac{\partial u}{\partial r} = \frac{\partial p}{\partial z} \cdot \frac{r}{2} = \frac{\Delta p}{t_{KH}} \cdot \frac{r_{ground} + r_{top}}{4} \tag{7}$$

The radius r is given by the average of the radius of the keyhole ground r_{ground} and the radius of the top of the keyhole r_{top}. The pressure gradient $\partial p/\partial z$ can be calculated by assuming a linear pressure difference Δp between the top and the bottom of the keyhole with a defined depth t_{KH}. For the calculation of Δp the values of the ablation pressure p_a at the bottom and the top of the keyhole have to be known. If geodetic and static pressure differences are neglected, the ablation pressure p_a can be calculated by:

$$p_a = \frac{\gamma}{r}, \tag{8}$$

where γ is the surface tension of the liquid metal and r the radius of the keyhole. Calculating the ablation pressure at the bottom p_{ground} and the top p_{top} of the keyhole by equation (7), the pressure difference Δp is given by:

$$\Delta p = p_{ground} - p_{top} = \gamma \left(\frac{1}{r_{ground}} - \frac{1}{r_{top}} \right) \tag{9}$$

Using equations (7) and (9) the shear-stress τ can be calculated and implemented at the boundary of the keyhole as a weak contribution in the equation of the conservation of momentum (2).

4.3. Model dimension and mesh

The model consists of a cuboid with a length of 20 mm, a width of 10 mm and a height of 5 mm. The keyhole is predefined and consists of a frustum for the body and a half-sphere for the ground. The frustum has an upper radius of r_{top}. The radius on the ground of the frustum is $r_{ground} = 0.2 \cdot r_{top}$, which also defines the radius of the half sphere. The complete depth of the keyhole is named t_{KH}. For meshing, the model is partitioned in two areas. Both are meshed with unstructured tetrahedron elements. While the area around the keyhole has a fine mesh with a minimal element size of 0.07 mm and a maximal element size of 0.38 mm, the remaining area of the model has a coarse mesh, which fulfils the requirements for the heat transfer calculation in the solid phase.

4.4. Boundary Conditions

Using boundary conditions, the energy input as well as the welding velocity can be implemented in the model. In Figure (1) the assignment of the boundary numbers in the model as well as the related boundary conditions are shown.

Number	Boundary	Velocity	Temperature
1	Inflow	$\vec{u} = \overrightarrow{v_0}$	T = 293 K
2	Outflow	Hydrostatic pressure	$-\vec{n} \cdot (\lambda \nabla T) = 0$
3, 4, 5, 6	Lateral surfaces	$\vec{u} \cdot \vec{n} = 0$	$-\vec{n} \cdot (\lambda \nabla T) = 0$
7	Keyhole surface	$\vec{u} \cdot \vec{n} = 0$	$T = T_V$

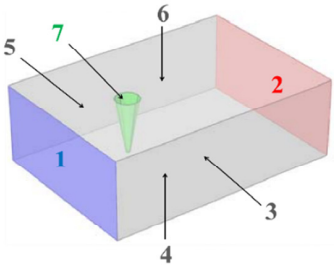

Fig. 1. Boundary conditions for the numerical model (left) and the assignment of the boundary numbers in the model (right).

To consider the welding velocity, the boundary 1 is defined as an inflow with a prescribed velocity. The temperature of this boundary is set to the ambient temperature. At boundary 2, defined as an outflow, a hydrostatic pressure is assumed. No material flow and no heat transfer perpendicular to the surface are permitted at boundaries 3 – 6. The energy is applied by a temperature constraint at the surface of the keyhole. Therefore, the boundary 7 is set to the evaporation temperature T_V of the copper material.

4.5. Material data

Table 1. Material properties of copper used in the simulation (l = liquid, s = solid) [14], [15].

Material property	Value	Unit
Melting temperature T_M	1357	K
Evaporation temperature T_V	2833	K
Density in the solid phase ρ_s	8960	kg m^{-3}
Density in the liquid phase ρ_l at $T = T_M$	8000	kg m^{-3}
Expansion coefficient α	-0.609	kg m^{-3} K^{-1}
Latent heat h_M	207	kJ kg^{-1}
Specific heat capacity in the solid phase $c_{p,s}$	385	J kg^{-1} K^{-1}
Specific heat capacity in the liquid phase $c_{p,l}$	473	J kg^{-1} K^{-1}
Thermal conductivity λ	394	W m^{-1} K^{-1}
Surface tension coefficient γ at $T = T_V$	1.285	N m^{-1}
Gradient of the surface tension $\partial\gamma/\partial T$	-0.13	mN m^{-1} K^{-1}
Dynamic viscosity η_{Max} for $T < T_M$	500	Pa s
Dynamic viscosity η_0	0.3009	mPa s
Reaction number K	3666.8	K

The basic material properties used in the presented model are listed in Table 1. The thermal conductivity is assumed to be temperature-independent in the solid as well as in the liquid phase. To consider the latent heat during the phase change between the solid and the liquid phase, the specific heat capacity c_p is modified [16]. Therefore, the latent heat is added to the specific heat by a normal distribution over a temperature area of $2 \cdot \delta T$. Thus, the modified heat capacity is given by:

$$c_p(T) = \begin{cases} c_{p,s} + \dfrac{\exp\left(-\left(\dfrac{T - T_M}{\delta T}\right)^2\right)}{\sqrt{\pi} \cdot \delta T} \cdot h_M & T < T_M \\ c_{p,l} + \dfrac{\exp\left(-\left(\dfrac{T - T_M}{\delta T}\right)^2\right)}{\sqrt{\pi} \cdot \delta T} \cdot h_M & T \geq T_M, \end{cases} \tag{10}$$

where $c_{p,s}$ is the heat capacity in the solid phase, $c_{p,l}$ the heat capacity in the liquid phase and h_M the latent heat. The dynamic viscosity η is separated into two intervals:

$$\eta(T) = \begin{cases} \eta_{Max} & T < T_M \\ \eta_0 \cdot \exp(K/T) & T \geq T_M \end{cases} \tag{11}$$

For temperatures below the melting temperature T_M, the dynamic viscosity is fixed to the value η_{Max} to suppress fluid flow. For areas with temperatures above the melting temperature, the dynamic viscosity is described by an Arrhenius type equation, which considers the temperature-dependence using the reaction number K [14].

4.6. Determination of the thermal efficiency

To determine the thermal efficiency, first the isosurface at the melting temperature has to be calculated using the numerical model with a time dependent solver. It was shown, that steady state conditions are reached after a simulation time of 100 ms. The isosurface at the melting temperature can be identified using the solution of this state. This surface is projected onto a plane, which is perpendicular to the welding direction. This projection corresponds to the dimension of the molten pool, which can be obtained using a cross section. The absorbed power P has to be known to calculate the thermal efficiency by the use of equation (1). This power is calculated by an integration of the heat flow over the surface of the keyhole.

5. Results and Discussion

5.1. Validation of the model

In order to validate the numerical model, experimental analysis were carried out. The experimental set-up presented in GANSER ET AL. [17] was used to determine the thermal efficiency during laser welding of copper material CW008A. The reflected power of the laser radiation was evaluated using a radiation analyzer. The cross section area of the weld seam was measured to calculate the thermal efficiency.

The numerical model was calibrated in the next step. Therefore, the melting isotherm was identified as described above. The keyhole geometry was adapted in a stepwise fashion in width and depth to change the curve of the melt isotherm, until the best fit with the cross section from the experiment was achieved. Figure 2 shows the cross section of a weld seam, welded with P = 6 kW and v = 10 m/min (left), and the result of the calibration of the numerical model for these welding parameters (right).

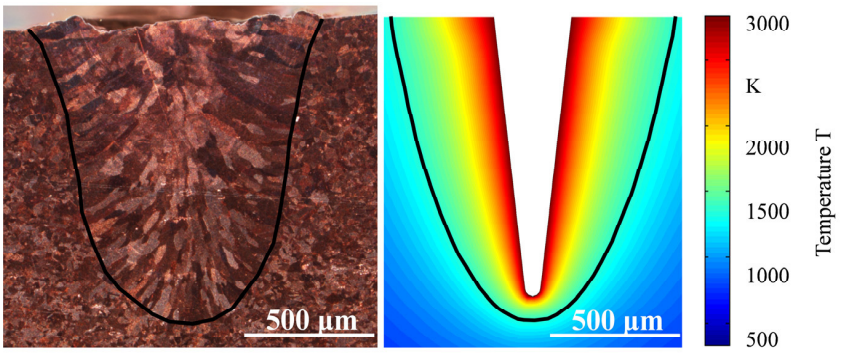

Fig. 2. Comparison of the melt isotherms of the welding process (left) and the numerical simulation (right) (P = 6 kW; v = 10 m/min).

After the calibration, the seam width, the welding depth, and the cross section were in good agreement to the experimental results (see Table 2). With respect to the thermal efficiency, the calculation based on the numerical model (see section 4.6) shows a close match to the experimental results of GANSER ET AL. [17].

Table 2. Results of the validation of the numerical model.

Measured variable	Experiment [17]	Numerical model
Absorbed laser power	2820 W	3070 W
Welding depth	1.19 mm	1.20 mm
Seam width	1.17 mm	1.10 mm
Cross section area	0.98 mm^2	0.93 mm^2
Thermal efficiency	0.29	0.28

5.2. Influence of the welding velocity and the keyhole geometry on the thermal efficiency

The influence of the welding velocity, the keyhole diameter and the keyhole depth on the thermal efficiency was analyzed using the presented numerical model. For this purpose, a full factorial design of simulation runs was carried out. The parameters for these investigations are listed in Table 3.

Table 3. Results of the validation of the numerical model.

Parameter	Values	Unit
Welding velocity	2, 4, 6, 8, 10	m/min
Keyhole diameter	100, 150, 200	µm
Keyhole depth	0.5, 1, 2, 3	mm

The dependence of the thermal efficiency on the welding velocity for different keyhole diameters is shown in Figure 3 (left). A strong increase of the efficiency for higher welding velocities can be observed. This figure also shows a small increase of the efficiency for an increasing focus diameter. All simulation runs shown in Figure 3 (left) were carried out at the same keyhole depth which explains these results. A smaller beam waist with the same laser power would lead to a deeper keyhole. Thus, the thermal efficiency would be increased, as shown in Figure 3 (right). A gain of the thermal efficiency can be identified at higher absorbed powers. This increase of the absorbed power happens because of an increased keyhole depth.

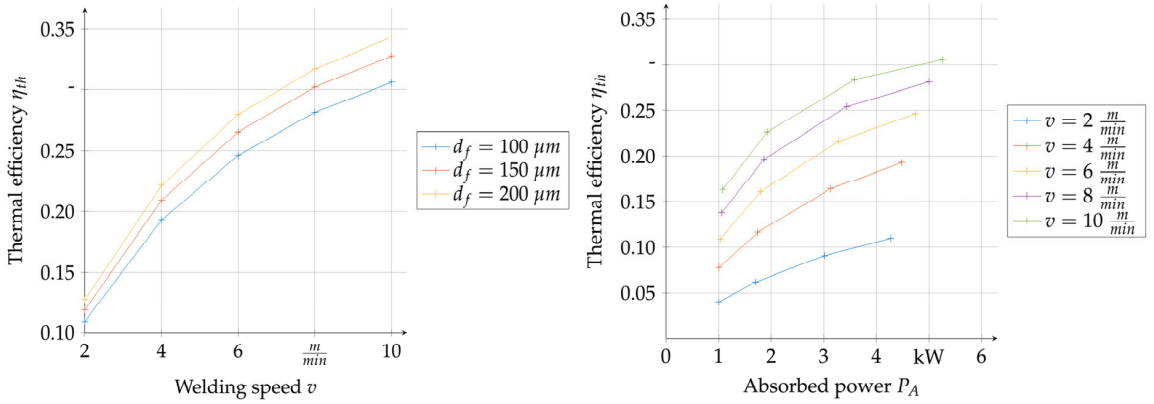

Fig. 3. Thermal efficiency over welding speed for an assumed keyhole depth of 0.5 mm (left) and the thermal efficiency over absorbed power for a focus diameter d_f = 200 µm (right). Associated results are connected by linear lines for illustration purposes.

6. Summary

A numerical model was presented, which enables the evaluation of the thermal efficiency during a laser deep penetration welding process. A CFD simulation was used to calculate the isosurface at the melting temperature of the metal. Based on this isosurface, the thermal efficiency was calculated. The fluid flow around a predetermined vapor capillary was considered as well as the thermal convection, the Marangoni convection and the convection driven by emerging metal vapor. Depending on the welding velocity and the geometry of the vapor capillary, the thermal efficiency was determined. It could be shown, that higher welding velocities and deeper vapor capillaries increase the thermal efficiency during keyhole welding.

Acknowledgements

This paper is based on investigations of the project ReLaTiS (“Transient spatial reflection of the laser beam during laser deep welding”), which is kindly supported by the German Research Foundation (DFG).

References

[1] Schulze, G., “Die Metallurgie des Schweissens: Eisenwerkstoffe - Nichteisenmetallische Werkstoffe“, Berlin: Springer (2010).

[2] Hess, A.; Schuster, R.; Heider, A.; Weber, R.; Graf, T.: “Continuous Wave Laser Welding of Copper with Combined Beams at Wavelengths of 1030nm and of 515nm.”, Physics Procedia 12, pp. 88-94, (2011).

[3] Rykalin, C., “Berechnung der Wärmevorgänge beim Schweissen.” Berlin: Verlag Technik (1957).

[4] Swift-Hook, D. T., Gick, A. E. F.: “Penetration welding with Lasers: Analytical study indicates that present laser beam welding capabilities may be extended tenfold.”, Welding Journal 52.11, pp. 492–499, (1973).

[5] Chang, C.-L.: “Berechnung der Schmelzbadgeometrie beim Laserstrahlschweissen mit Mehrfokustechnik”, Dissertation, University Stuttgart, München: Utz, (2000).

[6] Lee, J. Y.; Ko, S. H.; Farson, D. F.; Yoo, C. D.: “Mechanism of keyhole formation and stability in stationary laser welding”, Journal of Physics D: Applied Physics 35, pp. 1570–1576, (2002).

[7] Otto, A.; Koch, H.; Leitz, K.-H.; Schmidt, M.: “Numerical Simulations - A Versatile Approach for Better Understanding Dynamics in Laser Material Processing.” Physics Procedia 12, pp. 11–20, (2011).

[8] Zhang, L. J.; Zhang, J. X.; Gumenyuk, A.; Rethmeier, M.; Na, S. J.: “Numerical simulation of full penetration laser welding of thick steel plate with high power high brightness laser.”, Journal of Materials Processing Technology 214, pp. 1710–1720, (2014).

[9] Gatzen, M.; Tang, Z.: “CFD-based model for melt flow in laser beam welding of aluminium with coaxial magnetic field.” Physics Procedia 5, pp. 317–326, (2010).

[10] Bachmann, M.; Avilov, V.; Gumenyuk, A.; Rethmeier, M.: “Numerical simulation of full-penetration laser beam welding of thick aluminium plates with inductive support.”, Journal of Physics D: Applied Physics 45 3, pp. 35201, (2012).

[11] Hügel, H.; Graf, T.; „Laser in der Fertigung: Strahlquellen, Systeme, Fertigungsverfahren“, Wiesbaden: Springer (2014).

[12] Sahoo, P.; Debroy, T.; McNallan, M. J.: “Surface tension of binary metal - surface active solute systems under conditions relevant to welding metallurgy.”, Metallurgical Transactions B 19 3, pp. 483–491, (1988).

[13] Beck, M.: “Modellierung des Lasertiefschweissens”, Dissertation, University Stuttgart, Stuttgart: Teubner (1996).

[14] Poprawe, R.: “Lasertechnik für die Fertigung: Grundlagen, Perspektiven und Beispiele für den innovatioven Ingenieur.” Berlin: Springer, (2005).

[15] Haynes, W. M.: “CRC handbook of chemistry and physics.”, Boca Raton, Florida: CRC Press, (2014).

[16] Hu, H.; Argyropoulos, S. A.: “Mathematical modelling of solidification and melting.”, Modelling and Simulation in Materials Science and Engineering 4, pp. 371–396, (1996).

[17] Ganser, A.; Liebl, S.; Schmitz, P.; Zäh, M. F.: “Detection of transient reflections during laser beam welding of copper.”, Proc. of the conference on SPIE, 97410J. (2016).